A TEMPORAL APPROXIMATE DECONVOLUTION MODEL FOR LES

C. David Pruett and Benjamin C. Thomas
Department of Mathematics & Statistics,
James Madison University
Harrisonburg, Virginia 22807, USA
pruettcd@jmu.edu & thoma2bc@jmu.edu

Chester E. Grosch
Departments of Computer Science and Oceanography,
Old Dominion University
Norfolk, Virginia 23529, USA
grosch@cs.odu.edu

Thomas B. Gatski
Computational AeroSciences Branch,
NASA Langley Research Center
Hampton, Virginia 23681-2199, USA
thomas.b.gatski@nasa.gov

ABSTRACT

The approximate deconvolution model of Stolz and Adams (1999) has proven itself a practical and effective method for residual-stress modeling in large-eddy simulation. Innovative in many regards, the model is conventional in the sense that it exploits spatial filtering to separate resolved and unresolved scales of motion. On the other hand, although largely unexplored territory, time-domain filtering for large-eddy simulation offers both conceptual and practical advantages under certain circumstances. A natural question therefore arises: Can the approximate deconvolution model be adapted for time-domain filtering, and if so, how? The current paper explores one such approach. The particular temporal approximate deconvolution model developed herein exploits explicit time-domain filtering by means of a causal exponential filter expressed in differential form. The unavoidable phase error of causal filtering necessitates adaptations to the baseline (spatial) model. Specifically, both the residual-stress and secondary regularization components of the model require careful design to avoid instability. Proper design, however, appears to lead to a family of robust temporal approximate deconvolution models. The current model is demonstrated by temporal large-eddy simulation of plane-channel flow at nominal $Re_\tau = 180$ and $Re_\tau = 590$. These results are encouraging and suggest that the temporal model can perform on a par with the spatial approximate deconvolution model, thereby providing a viable alternative whenever circumstances warrant.

INTRODUCTION

A few years ago, Stolz and Adams (1999) unveiled an approximate deconvolution model (ADM) for large-eddy simulation (LES), which has performed well for flows as diverse as incompressible channel flow (Stolz et al., 2001a) and supersonic compression-ramp flow (Stolz et al., 2001b). In the ADM, the residual stress is approximated to arbitrarily high order by deconvolving (defiltering) the resolved-scale velocity fields $\bar{u}_j$. Specifically, the exact residual stress $R_{ij} \equiv \overline{u_i u_j} - \overline{u}_i \overline{u}_j$ is approximated as

$$\begin{aligned} M_{ij} &= \overline{v_i v}_j - \overline{v}_i \overline{v}_j \\ v_j &= \sum_{k=0}^{p} C_k \bar{u}_j^{(k+1)} \end{aligned} \tag{1}$$

The deconvolved velocity v_j approximates the unfiltered velocity u_j as a linear combination of (k-times) multiply filtered fields $\bar{u}_j^{(k)}$. The index p defines the *degree* of the deconvolution.

The coefficients C_k are derived indirectly from the transfer function $H(\xi)$ of the primary filter, where $\xi = \kappa\Delta$, κ is the wavenumber, and Δ is the spatial filter width. Provided the filter is invertible ($H \neq 0$) and $|1 - H| < 1$, the transfer function has an exact power-series inverse, namely $H^{-1} = \frac{1}{1-(1-H)} = \sum_{k=0}^{\infty}(1-H)^k$. The exact inverse, however, is undesirable for applications to LES, for only the resolved scales are of interest. Truncating the series at finite p yields the transfer function of the approximate inverse $\tilde{H}^{-1}$, namely

$$\tilde{H}^{-1} = 1+(1-H)+(1-H)^2+...+(1-H)^p = \sum_{k=0}^{p}(1-H)^k \tag{2}$$

By isometry between Fourier space (Eq. 2) and physical space (Eq. 1), the coefficients C_k of Eq. 1 are determined simply from the binomial theorem (i.e., from Pascal's triangle).

As a generalized scale-similarity model (Stolz and Adams, 1999), the ADM suffers from insufficient dissipation without secondary regularization (artificial viscosity) and tends toward numerical instability. Stabilization is accomplished by adding

a dissipative term to the right-hand sides of the momentum equations, namely

$$-\chi(\bar{u}_j - \bar{v}_j) \tag{3}$$

where χ is an arbitrary damping parameter. The Fourier-space analog of Eq. 3 is $-\chi(1 - H * \tilde{H}^{-1})H\hat{u}_j$, $\hat{u}_j$ being the Fourier coefficient of u_j. The relevant operator is $1 - H * \tilde{H}^{-1}$, which is purely real, and by means of which secondary regularization acts as a high-order, low-pass filter. (It is useful to distinguish here between deconvolution *degree* p, where $p+1$ simply defines the number of coefficients C_k, and *order*, which indicates the flatness of the operator at its origin. Specifically, the order of an operator in Fourier space corresponds to the first non-vanishing derivative of its modulus, evaluated at the origin.) Stolz et al. (2001a) show the secondary filter to have order $O[\Delta^{q*(p+1)}]$, where q is the order of the primary filter (in their case 4), and p is the deconvolution degree (in their case 5). Thus, in the original ADM, secondary regularization acts at extraordinarily high order (i.e., 24), functioning virtually as a spectral low-pass filter.

To summarize, in the original ADM, deconvolution serves two distinct purposes: 1) modeling of residual stress (Eq. 1), and 2) generation of high-order artificial viscosity (Eq. 3).

Relative to conventional spatial filtering, time-domain filtering for LES (hereafter TLES) offers certain conceptual and practical advantages (Dakhoul and Bedford, 1986, and Pruett, 2000) that have not previously received full consideration. Principal among these is that TLES affords a natural bridge between direct numerical simulation (DNS) and Reynolds-averaged Navier-Stokes (RANS) methodologies. The efficacy of TLES rests upon the premise that the removal of high-frequency content from the frequency spectrum should effectively remove high-wavenumber content from the wavenumber spectrum as well, so that TLES can be conducted at coarser temporal *and* spatial resolution than DNS.

In Pruett et al. (2003) the viability of TLES was established for viscous Burger's flow (at low Reynolds number to avoid shocks); however, it has remained to demonstrate the approach for three-dimensional flow. In this paper, we develop a temporal variant of the ADM, the "TADM," describe modifications necessary to adapt approximate deconvolution from spatial to temporal filtering, and present results of TLES for channel flow.

TEMPORAL APPROXIMATE DECONVOLUTION MODEL

Let $f(t)$ be any continuous function of time t. A causal linear filter is readily constructed by the integral operator

$$\bar{f}(t;\Delta) = \int_{-\infty}^{t} G(\tau - t;\Delta) f(\tau) d\tau \tag{4}$$

where G is a parameterized *filter kernel*, its parameter Δ is termed the (temporal) *filter width*, and an overline denotes a temporally filtered quantity. For admissibility, the kernel G must be non-negative, must be appropriately normalized, and must tend toward a Dirac delta function in the limit of vanishing filter width.

The exponential kernel, among many, satisfies the requisite conditions. Specifically, $G(t;\Delta) = 1/\Delta \exp(t/\Delta)$ yields the integral filter operator

$$\bar{f}(t;\Delta) = \frac{1}{\Delta}\int_{-\infty}^{t} \exp\left(\frac{\tau - t}{\Delta}\right) f(\tau) d\tau \tag{5}$$

whose transfer function is

$$H(\Omega) = \frac{1}{1 + i\Omega} \tag{6}$$

where $\Omega = \omega\Delta$, and ω is the circular frequency (Fig. 1).

An advantage of the exponential kernel is that the integral form (Eq. 5) has an equivalent differential form. That is, differentiation of Eq. 5 by Leibniz' rule yields the linear ODE

$$\frac{\partial \bar{f}}{\partial t} = \frac{f - \bar{f}}{\Delta} \tag{7}$$

for the filtered quantity $\bar{f}$. For reasons to become apparent, in the TADM, explicit filtering is imposed via the differential form of the operator. In its discrete implementation, Eq. 7 is naturally parameterized by the filter-width ratio $r = \Delta/\Delta t$ (Fig. 2).

Although the residual-stress model of the TADM is *formally* identical to Eq. 1, the adaptation to temporal filtering necessitates two modifications: 1) overlines denote temporally rather than spatially filtered quantities, and 2) the values of the coefficients C_k in Eq. 1 must be altered (the subject of the next section). By appending the Navier-Stokes equations (NSE) with an auxiliary set of evolution equations for the multiply-filtered velocity fields $\bar{u}_j^{(k)}$, we obtain the closed system

$$\begin{aligned}
\frac{\partial \bar{u}_j}{\partial x_j} &= 0 \\
\frac{\partial \bar{u}_i}{\partial t} + \frac{\partial(\bar{u}_i\bar{u}_j)}{\partial x_j} &= -\frac{\partial \bar{p}}{\partial x_i} + \frac{1}{Re}\frac{\partial^2 \bar{u}_i}{\partial x_j \partial x_j} - \frac{\partial M_{ij}}{\partial x_j} \\
M_{ij} &= \overline{v_i v_j} - \bar{v}_i\bar{v}_j \\
v_i &= \sum_{k=0}^{p} C_k \bar{u}_i^{(k+1)} \\
\frac{\partial}{\partial t}\bar{u}_i^{(k+1)} &= \frac{\bar{u}_i^k - \bar{u}_i^{(k+1)}}{\Delta} \ (1 \le k \le p) \\
\frac{\partial \bar{v}_i}{\partial t} &= \frac{v_i - \bar{v}_i}{\Delta} \\
\frac{\partial}{\partial t}(\overline{v_i v_j}) &= \frac{v_i v_j - \overline{v_i v_j}}{\Delta}
\end{aligned} \tag{8}$$

Certain advantages of the differential form of the filter are now apparent. First, the governing system is explicitly parameterized by the filter width Δ. Second, the entire system, including the model, can be advanced forward in time consistently by the same numerical integration scheme.

Although it appears that the computational overhead of the TADM is significant, the burden is relatively modest because of the simplicity and linearity of the additional evolution equations. The chief computational burden of the TADM is storage rather than CPU time. However, the memory saved by grid coarsening more than compensates for that lost to new variables.

It was shown in Pruett et al. (2003) that the parameterized system tends toward the NSE in the limit of vanishing filter width, and (for stationary flows) toward the RANS equations in the limit of infinite Δ, provided the model is exact. For finite p, the TADM is inexact, which places practical limitations on Δ (or r).

It remains to determine an appropriate degree p, filter-width ratio r, and coefficients C_k. For the ADM, a single set

of coefficients suffices both for residual-stress modeling and for secondary regularization. Because of the phase error (Fig. 1) associated with causal filters, however, two distinct sets of coefficients are prescribed for the TADM: one set (C_k) optimized for the residual-stress model, the other (D_k) for secondary regularization. The next two subsections derive the two coefficient sets, respectively, for $p = 3$.

Residual-Stress Model Coefficients

In Fourier space, the approximate deconvolution operator is $\tilde{H}^{-1} = \sum_{k=0}^{p} C_k H^k$, in which case the Fourier coefficients of u_j and v_j are related by $\hat{v}_j = H * \tilde{H}^{-1}\hat{u}_j$. For application to LES, the ideal shape of the modulus of $|H * \tilde{H}^{-1}|$ is that of a spectral (sharp cutoff) low-pass filter, in which case low frequency content is recovered faithfully, while high-frequency content is completely attenuated.

The binomial coefficients proposed for the ADM are unsuitable for the TADM. Due to the phase error of causal filters, energy at moderate frequency is amplified rather than attenuated. Thus, for the TADM the coefficients C_k must be expressly designed to give $|H * \tilde{H}^{-1}|$ "near-ideal" properties.

For specificity, consider third-degree deconvolution (i.e., $p = 3$). The parameter space consists initially of four free parameters: $[C_0, C_1, C_2, C_3]$. The normalization constraint, which requires the coefficients to sum to unity, reduces the parameter space by one. Without loss of generality, $C_3 = 1 - C_0 - C_1 - C_2$.

A further consideration involves the coefficient C_0. Unlike spatial filters (for example, the Padé filter whose transfer function is shown in Fig. 3), the transfer functions of causal filters do not vanish identically beyond the Nyquist frequency $\Omega = \pi$. Rather, they tend toward zero asmyptotically (e.g., Eq. 6). Consequently, as $\Omega \to \infty$, the deconvolution operator $H * \tilde{H}^{-1}$ decays slowly, as $1/\Omega$ if $C_0 \neq 0$, and as $1/\Omega^2$ if $C_0 = 0$. Because faster attenuation of high frequencies is highly desirable, C_0 is intentionally set to zero. From a physical point of view, $C_0 = 0$ implies that the deconvolved velocity is re-constructed only from fields that have been low-pass filtered at least twice. This ensures that high frequencies are not generated during deconvolution.

There remain two free parameters: C_1 and C_2. These are determined by forcing the second and fourth derivatives of $|H * \tilde{H}^{-1}|$ to zero to give the operator the desired low-pass character in Fourier space. (Odd-ordered derivatives are naturally zero.) Algebraic constraint equations are readily derived by use of computer algebra software. In general, the resulting equations are nonlinear and admit multiple solutions. Conjugate-symmetric complex solutions are discarded because they cannot be easily implemented in physical space. The remaining real solutions yield approximate inverses $\tilde{H}^{-1}$ that share the same moduli while differing in phase. In particular, for $p = 3$, the method described herein yields two real and two complex solutions, from which the following set of real coefficients is selected as optimal: $[0.0, \sqrt{6}, \sqrt{4 + 2\sqrt{6}} - 2\sqrt{6}, 1 - \sqrt{4 + 2\sqrt{6}} + \sqrt{6}]$. Figure 4 presents the moduli of H, $\tilde{H}^{-1}$, and $H * \tilde{H}^{-1}$ for this coefficient set.

Clearly the method can be extended to higher degree deconvolution. To date, deconvolution degrees of 2, 3, 4, and 5 have been examined, as have a variety of deconvolution coefficient sets and filter widths. In all cases, the instantaneous and mean residual stresses are well defined, with mean components that have qualitatively correct profiles. In sum, temporal deconvolution appears to admit a family of robust residual-stress models.

Secondary Regularization Coefficients

Secondary regularization in the TADM serves to impose high-order artificial viscosity to attenuate high frequencies that arise from numerical noise, while leaving the desired low frequencies relatively undisturbed.

Consider the complex exponential function $\hat{u}(t) = e^{i\omega t}$, which satisfies the differential equation of a harmonic oscillator, namely $\frac{d\hat{u}}{dt} = i\omega\hat{u}$. Secondary regularization functions as a dissipative term for the harmonic oscillator. Accordingly, consider the model problem

$$\frac{d\hat{u}}{dt} = i\omega\hat{u} - \chi(\hat{u} - \hat{v}) = [i\omega + \chi(H * \tilde{H}^{-1} - 1)]\hat{u} \qquad (9)$$

The dissipative term, the Fourier-space analog of Eq. 3, imposes exponential damping provided $Re[i\omega + \chi(H * \tilde{H}^{-1} - 1)] < 0.0$ which is satisfied if and only if

$$\lambda(\Omega) \equiv \chi Re(H * \tilde{H}^{-1} - 1) < 0.0 \qquad (10)$$

where the damping parameter $\chi > 0$ scales the exponential decay rate $\lambda(\Omega)$.

Equation 10 is violated whenever the binomial coefficients are used for secondary regularization of the TADM, leading to exponential growth in time at some frequencies. For a given degree p, optimal coefficients can be found conveniently by setting derivatives of $\mathrm{Re}[H * \tilde{H}^{-1}]$ to zero, which, once again, is accomplished via computer algebra software. For example, for $p = 3$, there remain three free parameters after normalization. Optimal coefficients are found by forcing the second, fourth, and sixth derivatives of $\mathrm{Re}[H * \tilde{H}^{-1}]$ to zero. (Again, odd-order derivatives vanish naturally.) Specifically, the optimal coefficients for third-order temporal secondary regularization are $[D_0, D_1, D_2, D_3] = [\frac{35}{16}, \frac{-29}{16}, \frac{3}{4}, \frac{-1}{8}]$. The decay rate λ for this coefficient set is shown in Fig. 5 for $\chi = 1$. Similarly, an optimal set of coefficients for second-order ($p = 2$) secondary regularization is $[D_0, D_1, D_2] = [\frac{15}{8}, \frac{-9}{8}, \frac{1}{4}]$. Figure 5 also presents λ for the $p = 2$ scenario.

In summary, for the current TADM, the order of the primary deconvolution is $2p$, while that of the secondary filter is $2(p + 1)$. For degree $p = 3$, for example, the primary and secondary deconvolutions are of orders 6 and 8, respectively. A more consistent approach would perhaps blend degree $p+1$ primary with degree p secondary deconvolution. Of moderately high order, secondary deconvolution for the TADM nonetheless acts at much lower order than the near-spectral order of the baseline ADM secondary operator. The effect of lower order secondary regularization on flow physics is unknown. Although it has been demonstrated that temporal secondary regularization is a viable approach to stabilizing the TADM, there may be other viable or preferable options.

RESULTS

The efficacy of TLES is demonstrated by simulating plane channel flow at nominal values Re_τ of 180 and 590. Channel flow has been studied extensively by DNS, and a high-quality statistical database exists for purposes of validation (Moser et al., 1999). Moreover, channel flow has been investigated by Stolz et. al. (2001a), who use LES methodology with

Table 1: Summary of test cases at nominal $Re_\tau = 180$.

Case	p	(r, χ)	Re_τ	model
TLES180a	N/A	N/A	203.0	none
TLES180b	3	(8,1.0)	195.4	TADM
TLES180c	3	(8,2.0)	193.5	TADM
TLES180d	2	(8,1.0)	189.8	TADM
TLES180e	2	(12,1.0)	176.4	TADM
SAK180a	N/A	N/A	173.	ADM

the ADM. Henceforth the DNS and ADM reference results will be referred to by the initials of their investigators, MKM and SAK, respectively. The DNS, LES, and TLES simulations each exploit efficient pseudospectral numerical methods in space; the latter two simulations employ the code TRANSIT of Gilbert and Kleiser, which is documented in Sandham and Kleiser (1992).

For all TLES results presented herein, the flow is initialized to a randomly perturbed laminar state, allowed to transition, and then permitted to settle into a stationary state prior to the acquisition of turbulent statistics.

Nominal $\mathbf{Re_\tau = 180}$

Table 1 summarizes the TLES test cases at nominal $Re_\tau = 180$. For all cases, the bulk Reynolds number was specified at $Re_{\text{bulk}} = 2800$. On the other hand, Re_τ is a statistic of the flow, for which the correct reference value is assumed to be that of the DNS, namely $Re_\tau = 178.1$. Whereas the reference DNS required a spatial grid resolution of 128^3, the reference LES and TLES were conducted at 32^3 resolution. Because the temporal resolution of the TLES was also 4 times coarser than that of the DNS, the aggregate reduction factor in computational workload relative to DNS was roughly 100 (after the overhead of the model was considered).

All TLES cases were conducted with the optimized model coefficients C_k derived for $p = 3$ in the previous section. Cases are distinguished by their particular values of filter-width ratio r and damping parameter χ, as specified in Table 1. Secondary regularization was accomplished with coefficients D_k for $p = 2$ or $p = 3$, also as indicated in the table.

In summary, all TLES simulations improve upon the no-model case (TLES180a), for which $Re_\tau = 203$. The best results, from Case TLES180e, yield a computed Re_τ with just one percent error. As expected, the solution is relatively insensitive to the arbitrary damping parameter χ, as reported also for the ADM (Stolz et al., 2001a). Figure 6 presents mean streamwise velocity profiles for cases TLES180a (no-model) and TLES180e (optimal) relative to the DNS results of Moser et al. (1999). Clearly the model, properly tuned, is effective. It should be kept in mind that $Re_\tau = 180$ represents in some sense an extreme test of TLES because barely turbulent wall-bounded flow is highly anisotropic (Fig. 7). Moreover, present results with the TADM should be considered suboptimal, because the parameter space of the model has not yet been fully explored.

Nominal $\mathbf{Re_\tau = 590}$

Table 2 and Figs. 8-11 summarize the TLES test and reference cases at nominal $Re_\tau = 590$, for which $p = 3$ for both the primary and secondary deconvolutions. For all simulations $Re_{\text{bulk}} = 10935$.

Table 2: Summary of test and reference cases at nominal $Re_\tau = 590$.

Case	$N_x \times N_y \times N_z$	Δt	Re_τ	model	(r, χ)
MKM	$384 \times 384 \times 257$	—	587	none	NA
SAK	$48 \times 64 \times 65$	—	574	ADM	NA
TLES	$48 \times 64 \times 65$	0.04	595	TADM	(8,1.0)

Figures 8 and 9 present time evolution of instantaneous Re_τ and turbulent kinetic energy k, respectively, for TLES. Note that TLES is sufficiently robust to survive the strong peak in k associated with transition and that the model $k_R[= 0.5M_{ii}]$ responds appropriately. The computed mean Re_τ for the TLES of 595 is just over one percent in error relative to the reference value of 587. Further, Fig. 10 shows reasonably good agreement of the mean streamwise velocity with DNS results. Finally, Fig. 11 presents selected components of Reynolds stress relative to their DNS counterparts, where the sum $\bar{\tau}_{ij} + < M_{ij} >$ directly approximates the exact residual stress τ_{ij}, and $\bar{\tau}_{ij}$ is the resolved-scale Reynolds stress.

ACKNOWLEDGMENTS

The authors are grateful to L. Kleiser and P. Schlatter of ETH Zurich for permission to use the channel-flow simulation code TRANSIT and for guidance in its implementation.

REFERENCES

Dakhoul, Y. M., and Bedford, K. W., 1986, "Improved Averaging Method for Turbulent Flow Simulation. Part I: Theoretical Development and Application to Burger's Transport Equation," *International Journal for Numerical Methods in Fluids*, Vol. 6, No. 2, pp. 49-64.

Moser, R. D., Kim, J., and Mansour, N. N., 1999, "Direct Numerical Simulation of Turbulent Channel Flow up to $Re_\tau = 590$," *Physics of Fluids*, Vol. 11, No. 4, pp. 943-945.

Pruett, C. D., 2000, "On Eulerian Time-Domain Filtering for Spatial Large-Eddy simulation," *AIAA Journal*, Vol. 38, No. 9, pp. 1634-1642.

Pruett, C. D., Gatski, T. B., Grosch, C. E., and Thacker, W. D., 2003, "The Temporally Filtered Navier-Stokes Equations: Properties of the Residual Stress," *Physics of Fluids*, Vol. 15, No. 8, pp. 2127-2140.

Sandham, N. D., and Kleiser, L., 1992, "The Late Stages of Transition to Turbulence in Channel Flow," *Journal of Fluid Mechanics*, Vol. 245, pp. 319-347.

Stolz, S., and Adams, N. A., 1999, "An Approximate Deconvolution Procedure for Large-Eddy Simulation," *Physics of Fluids*, Vol. 11, No. 7, pp. 1699-1701.

Stolz, S., Adams, N. A., and Kleiser, L., 2001a, "An Approximate Deconvolution Model for Large-Eddy Simulations with Application to Incompressible Wall-Bounded Flows," *Physics of Fluids*, Vol. 13, No. 4, pp. 997-1015.

Stolz, S., Adams, N. A., and Kleiser, L., 2001b, "An Approximate Deconvolution Model for Large-Eddy Simulations of Compressible Flows and its Application to Shock-Turbulent-Boundary-Layer Interaction," *Physics of Fluids*, Vol. 13, No. 10, pp. 2985-3001.

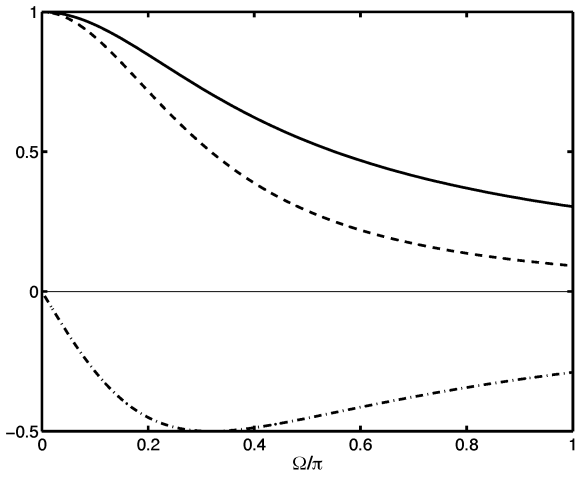

Figure 1: Transfer function of causal exponential filter. LEGEND: $|H(\Omega)|$ (solid); $H_r(\Omega)$ (dashed); $H_i(\Omega)$ (dashed-dotted).

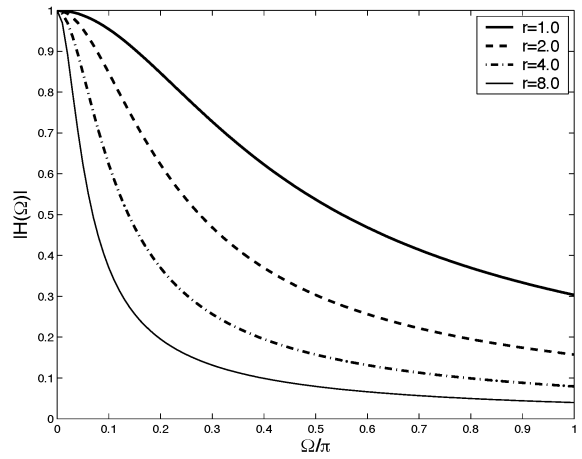

Figure 2: Transfer function of parameterized exponential filter.

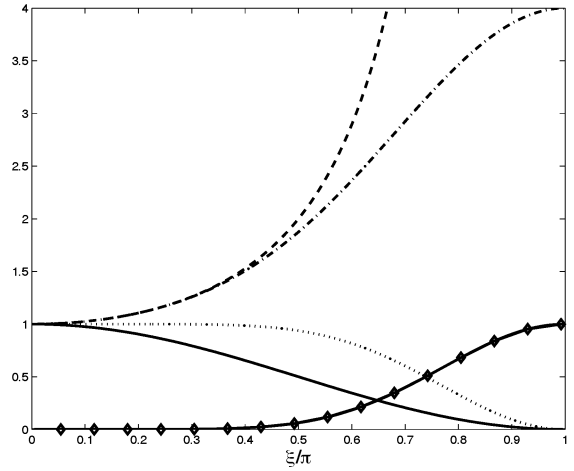

Figure 3: 2nd-order Padé spatial filter and related operators for $p = 3$. LEGEND: H (solid), exact H^{-1} (dashed), $\tilde{H}^{-1}$ (dashed-dotted), $H*\tilde{H}^{-1}$ (dotted), and $1-H*\tilde{H}^{-1}$ (symbols).

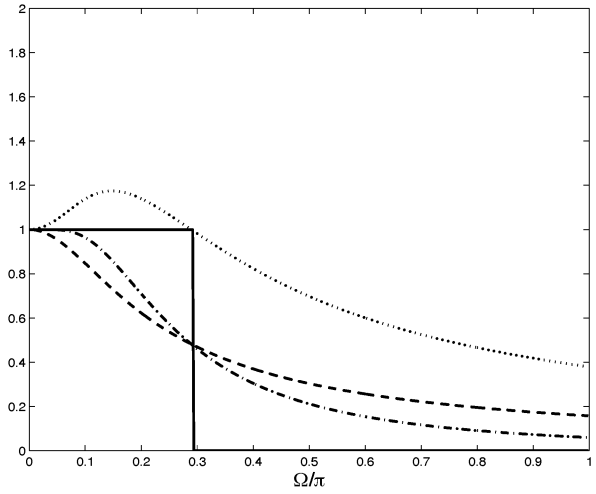

Figure 4: 3rd-degree temporal deconvolution with optimized coefficients and $r = 2$. LEGEND: $|H|$ (dashed), $|\tilde{H}^{-1}|$ (dotted), $|H*\tilde{H}^{-1}|$ (dashed and dotted), and spectral ideal (solid).

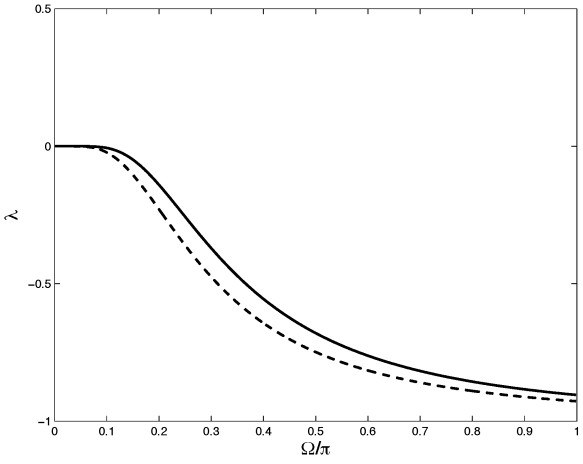

Figure 5: Exponential decay rate $\lambda(\Omega)$ for temporal secondary regularization operators with optimized coefficients D_k, for $r = 2$ and $\chi = 1.0$. LEGEND: $p = 3$ (solid); $p = 2$ (dashed).

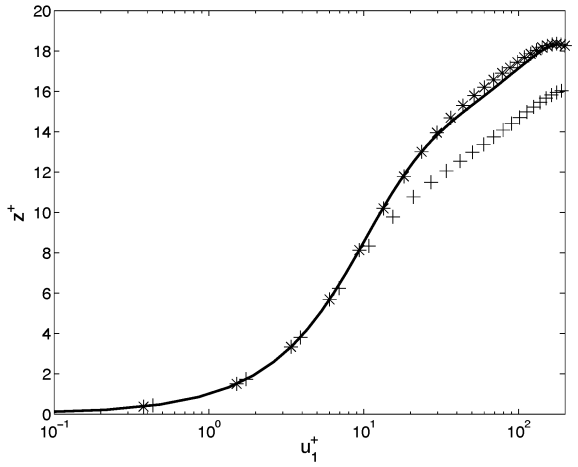

Figure 6: Mean streamwise velocity u_1 vs wall-normal coordinate z, in wall units. LEGEND: DNS (solid); no-model case TLES180a (plus symbol); TLES180e (asterisk).

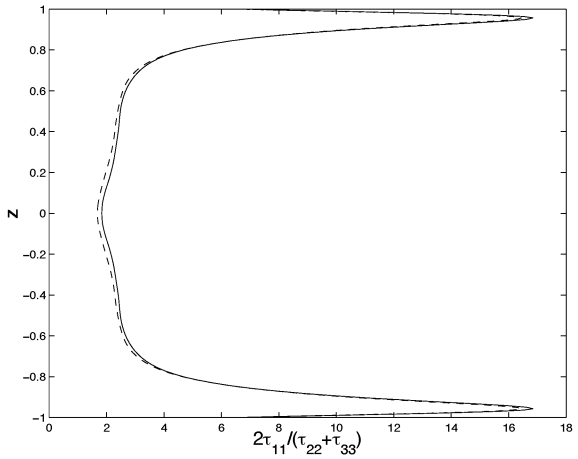

Figure 7: Measure of extreme near-wall anisotropy in channel flow at nominal $Re_\tau = 180$. LEGEND: Reference DNS of KMM (solid); DNS using TRANSIT (dashed).

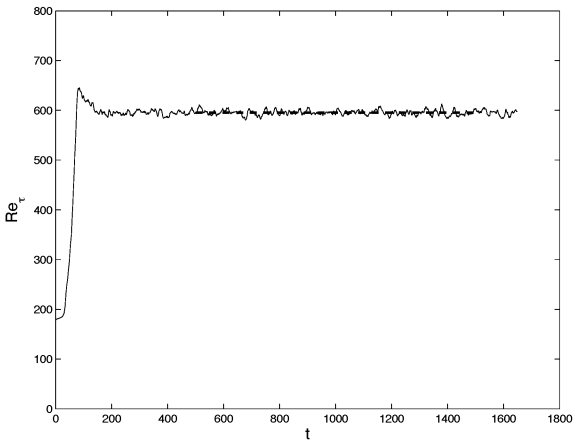

Figure 8: Evolution of instantaneous Re_τ (solid) and its mean (dashed) over $500 \leq t \leq 1500$ for Case TLES590.

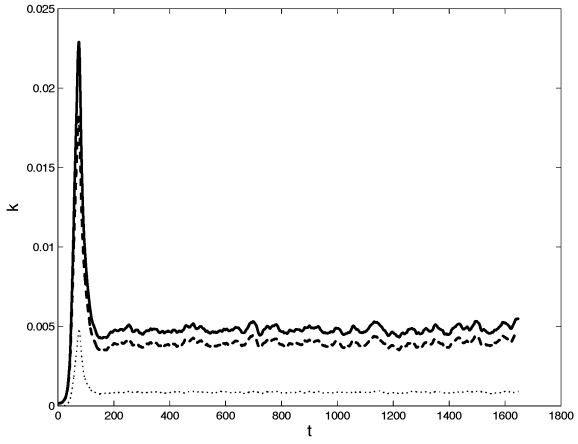

Figure 9: Turbulent kinetic energy for Case TLES590. LEGEND: instantaneous k (heavy solid); $\bar{k}[= 0.5\bar{\tau}_{ii}]$ (heavy dashed); $k_R[= 0.5M_{ii}]$ (dashed).

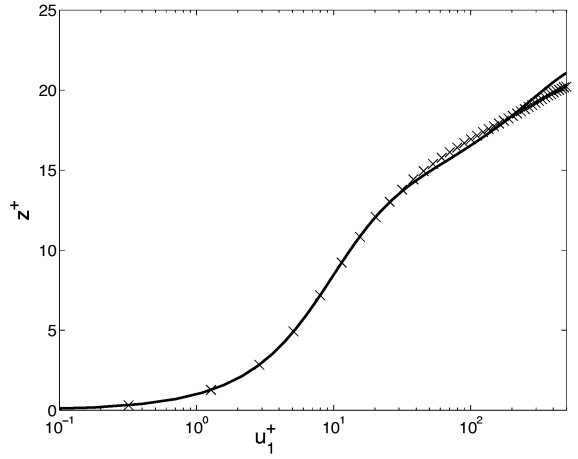

Figure 10: Mean streamwise velocity u_1 vs. wall-normal coordinate z, in wall units. LEGEND: DNS (solid); TLES590 (symbols, indicating grid points).

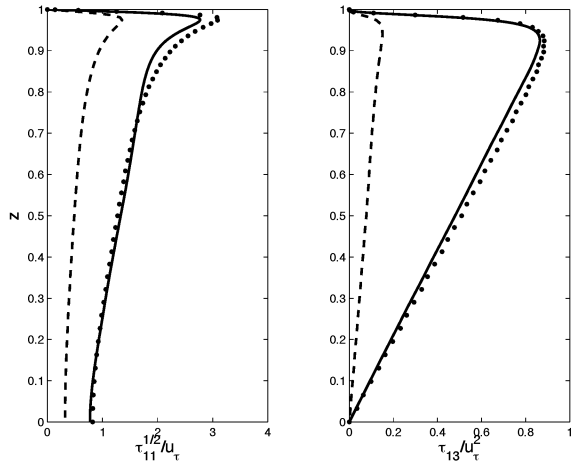

Figure 11: Reynolds stress. LEGEND: DNS (solid); TLES590 (symbols); $< M_{ij} >$ (dashed).